ELSEVIER

Computational Materials Science 16 (1999) 70–75

COMPUTATIONAL MATERIALS SCIENCE

# Quantitative prediction of effective material properties of heterogeneous media

J. Widjajakusuma [a,*], B. Biswal [a,b], R. Hilfer [a,c]

[a] *ICA-1, Universität Stuttgart, Pfaffenwaldring 27, 70569 Stuttgart, Germany*
[b] *Department of Physics and Electronics, Sri Venkateswara College, University of Delhi, New Delhi 110 021, India*
[c] *Institut für Physik, Universität Mainz, 55099 Mainz, Germany*

**Abstract**

Effective electrical conductivity and electrical permittivity of water-saturated natural sandstones are evaluated on the basis of local porosity theory (LPT). In contrast to earlier methods, which characterize the underlying microstructure only through the volume fraction, LPT incorporates geometric information about the stochastic microstructure in terms of local porosity distribution and local percolation probabilities. We compare the prediction of LPT and of traditional effective medium theory with the *exact* results. The exact results for the conductivity and permittivity are obtained by solving the microscopic mixed boundary value problem for the Maxwell equations in the quasistatic approximation. Contrary to the predictions from effective medium theory, the predictions of LPT are in better quantitative agreement with the exact results. 

*Keywords:* Porous materials; Effective material parameters; Self-consistent method

## 1. Introduction

Almost all discussions of mechanical properties, (e.g. elasticity, plasticity, viscoelasticity or fracture) and transport properties, (e.g. thermal conductivities, electric conductivities or diffusion constants) of microscopically heterogeneous materials assume that the material is homogeneous on a sufficiently macroscopic length scale [1,3,6,7,11,14–16]. Although there are different methods to describe random microstructures (e.g. see [10]), the macroscopic mechanical or transport parameters in most applicable theories depend on random microstructure solely through a single parameter, namely the volume fraction.

Microstructures are often very complicated and this complexity cannot be captured by a single parameter. To see this intuitively, consider a two-phase medium composed of 50% rubber and 50% steel. Two possible cases arise: (a) disconnected rubber inclusions are embedded in the connected steel matrix, and (b) disconnected steel particles are spread in the connected rubber matrix. Although it is clear that the first medium has very different elastic properties than the second one, a calculation of effective elastic constants including only the volume fraction would fail to bring out this distinction.

Difficulties of this nature have led to the need for theories that incorporate more quantitative information about the underlying microstructure. Recently a general method, namely local porosity

* Corrsponding author.

0927-0256/99/$ - see front matter 
PII: S0927-0256(99)00047-6

theory (LPT), was proposed [2,8–10]. It provides quantitative geometric characteristic functions through which microscopic pore spaces of real sandstones and models can be compared. It also provides a theoretical framework which incorporates these functions into the determination of the effective transport parameters. We have carried out an analysis on two different natural sandstones and obtained encouraging results which we report here.

The organisation of the paper is as follows. In Section 2 we present the samples and their conventional characterization theory by means of porosity and correlation function. In Section 3 we define the geometric characterization of LPT. Section 4 provides the definition of the effective material parameters and the general mixing-law based on LPT. This mixing-law contains the classical mixing-formulae, such as Bruggeman's effective medium equation or Clausius–Mossotti approximation [3,10,16], as special cases. In Section 5 we present the results and conclusion.

## 2. Porosity and correlation functions

Consider a rock sample occupying a subset $\mathbb{S} \subset \mathbb{R}^d$ $(d = 3)$ that contains two disjoint subsets $\mathbb{S} = \mathbb{P} \cup \mathbb{M}$ with $\mathbb{P} \cap \mathbb{M} = \emptyset$ where $\mathbb{P}$ is the pore space and $\mathbb{M}$ is the rock or mineral matrix and $\emptyset$ is the empty set. The porosity $\phi(\mathbb{S})$ is defined as the ratio $\phi(\mathbb{S}) = \mathbb{V}(\mathbb{P})/\mathbb{V}(\mathbb{S})$ which gives the volume fraction of the pore space. Here $V(\mathbb{P})$ denotes the volume of the pore space, and $V(\mathbb{S})$ is the total sample volume.

For the sample data analysed here the set $\mathbb{S}$ is a rectangular parallelepiped whose sidelengths are $M_1, M_2$ and $M_3$ in units of the lattice constant $a$ (resolution) of a simple cubic lattice. The total number of voxels is

$N = M_1 M_2 M_3$, and

$$\chi_{\mathbb{G}}(\mathbf{r}) = \begin{cases} 1 & \text{for } \mathbf{r} \in \mathbb{G}, \\ 0 & \text{for } \mathbf{r} \notin \mathbb{G}, \end{cases} \tag{1}$$

is the characteristic (or indicator) function of a set $\mathbb{G}$ that indicates when a point is inside or outside of $\mathbb{G}$. The correlation function for a homogeneous medium is defined as

$$G(\mathbf{r}_0, \mathbf{r}) = G(\mathbf{r} - \mathbf{r}_0) = \frac{\langle \chi_{\mathbb{P}}(\mathbf{r}_0)\chi_{\mathbb{P}}(\mathbf{r})\rangle - \langle\phi\rangle^2}{\langle\phi\rangle(1 - \langle\phi\rangle)}, \tag{2}$$

where $\langle\cdots\rangle$ denotes the ensemble average. If the medium is isotropic $G(\mathbf{r}) = G(|\mathbf{r}|) = G(r)$, with $G(0) = 1$ and $G(\infty) = 0$.

In the present work we consider two natural sandstones (Berea and Fontaine-bleau). The data sets were obtained by computerized microtomography. The resolution $a$ of the discretization, the sidelengths $M_i$ of the sample, and the average porosity $\bar{\phi}$ for the two samples are listed in Table 1. The length scale $\hat{L}$ will be defined and discussed in Section 5. The corresponding two-point correlation functions for the two samples are shown in Fig. 1.

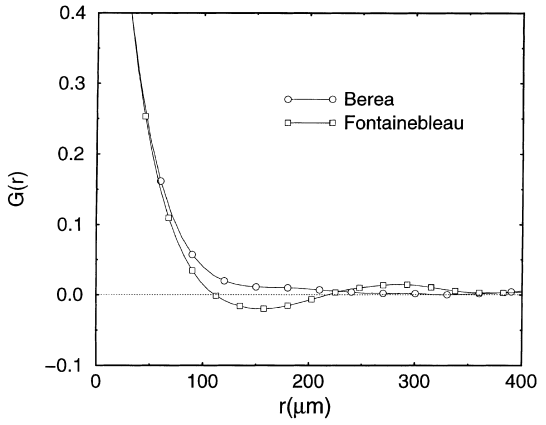


Fig. 1. The two-point correlation function $G(r)$ for the two samples of Berea (circles) and Fontainebleau (squares) sandstones with $G(0) = 1$.

Table 1
Resolution $a$, sidelengths $M_1, M_2, M_3$, average porosity $\bar{\phi}$ and a length scale $\hat{L}$ (see below) for the two sandstone samples

| Samples | $a$ (μm) | $M_1 \times M_2 \times M_3$ | $\bar{\phi}$ | $\hat{L}$ (μm) |
|---|---|---|---|---|
| Berea | 10 | $128 \times 128 \times 128$ | 0.1775 | 150 |
| Fontainebleau | 7.5 | $128 \times 128 \times 128$ | 0.1208 | 200 |

## 3. Local geometric characteristic functions

The basic idea of LPT is to measure geometric observables within a bounded (compact) subset of the porous medium and to collect these measurements into various histograms. Let $\mathbb{K}(\mathbf{r}, L)$ denote a cube of sidelength $L$ centered at the lattice vector $\mathbf{r}$. The set $\mathbb{K}(\mathbf{r}, L)$ defines a measurement cell inside which local geometric properties such as porosity or specific internal surface are measured. The local porosity within the cell $\mathbb{K}(\mathbf{r}, L)$ is defined as

$$\phi(\mathbf{r}, L) = \frac{V(\mathbb{P} \cap \mathbb{K}(\mathbf{r}, L))}{V(\mathbb{K}(\mathbf{r}, L))}. \tag{3}$$

The *local porosity distribution* $\mu(\phi, L)$ is defined as

$$\mu(\phi, L) = \frac{1}{m} \sum_{\mathbf{r}} \delta(\phi - \phi(\mathbf{r}, L)), \tag{4}$$

where $m$ is the number of placements of the measurement cell $\mathbb{K}(\mathbf{r}, L)$. Ideally all measurement cells should be disjoint, but in practice this cannot be achieved because of poor statistics. The results presented below are obtained by placing $\mathbb{K}(\mathbf{r}, L)$ on all lattice sites $\mathbf{r}$ which are at least a distance $L/2$ from the boundary of $\mathbb{S}$, and hence $m = \prod_{i=1}^{3}(M_i - L + 1)$. $\mu(\phi, L)$ is the empirical probability density function (histogram) of local porosities whose support is the unit interval.

Next the connectivity of a measurement cell needs to be characterized. Let

$$\Lambda(\mathbf{r}, L) = \begin{cases} 1 & \text{if } \mathbb{K}(\mathbf{r}, L) \text{ percolates in the} \\ & x\text{-, } y\text{- and } z\text{-direction,} \\ 0 & \text{otherwise,} \end{cases} \tag{5}$$

be an indicator for the connectivity of a cell. A cell $\mathbb{K}(\mathbf{r}, L)$ is called "percolating in the $x$-direction" if there exists a path inside the set $\mathbb{P} \cap \mathbb{K}(\mathbf{r}, L)$ connecting those two boundary faces of $\mathbb{S}$ that are vertical to the $x$-axis, similarly for the other directions.

The *local percolation probability* in all three directions is now defined through

$$\lambda(\phi, L) = \frac{\sum_{\mathbf{r}} \Lambda(\mathbf{r}, L) \delta_{\phi\phi(\mathbf{r}, L)}}{\sum_{\mathbf{r}} \delta_{\phi\phi(\mathbf{r}, L)}}. \tag{6}$$

The local percolation probability $\lambda(\phi, L)$ gives the fraction of measurement cells of sidelength $L$ with local porosity $\phi$ that are percolating in all three directions.

The *total fraction of percolating cells* is given by integration over all local porosities as

$$p(L) = \int_0^1 \mu(\phi, L)\lambda(\phi, L)\,\mathrm{d}\phi \tag{7}$$

and it characterizes the overall connectivity of the sample. Clearly $\lim_{L\to\infty} p(L) = 0$ if $\mathbb{P}$ is disconnected while $\lim_{L\to\infty} p(L) = 1$ if $\mathbb{P}$ is connected.

## 4. Effective permittivities

### 4.1. Definition

To demonstrate our method of calculating macroscopic material parameters we consider the problem of dielectric relaxation. Let $\mathbb{P}$ and $\mathbb{M}$ have the isotropic permittivities $\epsilon_{\mathbb{P}}$ and $\epsilon_{\mathbb{M}}$, respectively. The basic equations governing the static electric displacement $\mathbf{D}(\mathbf{r})$ in such a two-phase material are

$$\nabla \cdot \mathbf{D}(\mathbf{r}) = 0, \quad \mathbf{r} \in \mathbb{G} \ (\mathbb{G} = \mathbb{P}, \mathbb{M}). \tag{8}$$

The local constitutive equation is

$$\mathbf{D}(\mathbf{r}) = \epsilon(\mathbf{r})\mathbf{E}(\mathbf{r}), \tag{9}$$

where

$$\epsilon(\mathbf{r}) = \epsilon_{\mathbb{P}}\chi_{\mathbb{P}}(\mathbf{r}) + \epsilon_{\mathbb{M}}\chi_{\mathbb{M}}(\mathbf{r}). \tag{10}$$

Here $\mathbf{E}(\mathbf{r})$ is the electric field, which can be expressed as the gradient of the electric potential $U$, i.e. $\mathbf{E}(\mathbf{r}) = -\nabla U(\mathbf{r})$.

The effective permittivity $\epsilon_{\text{eff}}$ is defined as

$$\langle \mathbf{D}(\mathbf{r}) \rangle = \epsilon_{\text{eff}} \langle -\nabla U(\mathbf{r}) \rangle, \tag{11}$$

where angular brackets denote an ensemble average over the microstructure. Eq. (11) provides a relation between the averaged fields on the macroscopic level.

### 4.2. Mixing-law

In LPT, as in most of the classical effective medium approximations (EMA), it is assumed that the local geometries are statistically indepen-

dent, and simple enough to be modelled as spherical-coated inclusions embedded in an effective medium [6,16].

Consider a static electric field $\mathbf{E}_0 = E_0\,\mathbf{e}_z$ (in positive $z$-direction) incident on a sphere of radius $r_2$ (pore space) uniformly coated with spherical shell of radius $r_1$ (matrix) immersed in an effective medium with permittivity $\epsilon_{\text{eff}}$. In polar coordinates $(r,\theta,\varphi)$ the potential $U_{\text{out}}$ outside the coated sphere is given by an elementary result of electrostatics as [5,12]

$$U_{\text{out}}(r,\theta,\varphi) = -E_0\, r\cos\theta + \frac{\alpha}{r^2}\cos\theta. \tag{12}$$

Here

$$\alpha = r_1^3\,\frac{\epsilon_{\text{CS}}(\epsilon_{\mathbb{P}},\epsilon_{\mathbb{M}};\phi) - \epsilon_{\text{eff}}}{\epsilon_{\text{CS}}(\epsilon_{\mathbb{P}},\epsilon_{\mathbb{M}};\phi) + 2\epsilon_{\text{eff}}}E_0 \tag{13}$$

and $\phi = (r_2/r_1)^3$ is the local volume fraction.

The corresponding coated sphere permittivity can be expressed as

$$\epsilon_{\text{CS}}(\epsilon_{\mathbb{M}},\epsilon_{\mathbb{P}};\phi) = \epsilon_{\mathbb{M}}\left[\frac{\epsilon_{\mathbb{P}} + 2\epsilon_{\mathbb{M}} + 2\phi(\epsilon_{\mathbb{P}} - \epsilon_{\mathbb{M}})}{\epsilon_{\mathbb{P}} + 2\epsilon_{\mathbb{M}} - \phi(\epsilon_{\mathbb{P}} - \epsilon_{\mathbb{M}})}\right]. \tag{14}$$

If the materials are exchanged one obtains $\epsilon_{\text{CS}}(\epsilon_{\mathbb{P}},\epsilon_{\mathbb{M}};1-\phi)$ instead of $\epsilon_{CS}(\epsilon_{\mathbb{M}},\epsilon_{\mathbb{P}};\phi)$.

The self-consistency condition of the EMA requires that the average electric field $\langle\mathbf{E}(r,\theta,\varphi)\rangle$ equals the external field $E_0$, i.e. $\langle\mathbf{E}(r,\theta,\varphi)\rangle = \mathbf{E}_0$, within the effective medium. Substituting (12) into (11) and using this self-consistency condition, yields

$$\langle\alpha\rangle = 0, \tag{15}$$

where the $\langle\cdots\rangle$ indicates an average over $\phi$.

The mixing-law resulting from Eq. (15) reads

$$\int_0^1 \mu(\phi,L)\lambda(\phi,L)\frac{\epsilon_{\text{CS}}(\epsilon_{\mathbb{P}},\epsilon_{\mathbb{M}};1-\phi) - \epsilon_{\text{eff}}}{\epsilon_{\text{CS}}(\epsilon_{\mathbb{P}},\epsilon_{\mathbb{M}};1-\phi) + 2\epsilon_{\text{eff}}}\,\mathrm{d}\phi + \int_0^1 \mu(\phi,L)[1-\lambda(\phi,L)]\frac{\epsilon_{\text{CS}}(\epsilon_{\mathbb{M}},\epsilon_{\mathbb{P}};\phi) - \epsilon_{\text{eff}}}{\epsilon_{\text{CS}}(\epsilon_{\mathbb{M}},\epsilon_{\mathbb{P}};\phi) + 2\epsilon_{\text{eff}}}\,\mathrm{d}\phi = 0. \tag{16}$$

$\epsilon_{\text{CS}}(\epsilon_{\mathbb{P}},\epsilon_{\mathbb{M}};1-\phi)$ is the permittivity of the water-coated spherical rock grain and $\epsilon_{CS}(\epsilon_{\mathbb{M}},\epsilon_{\mathbb{P}};\phi)$ the permittivity of the rock-coated spherical water pore grain.

Because every EMA neglects the influence of local pore geometry, we emphasize that $\epsilon_{\text{eff}}$ calculated from Eq. (16) is an approximate effective permittivity.

## 5. Results and discussion

In Fig. 2 we present the local porosity distribution and the local percolation probability functions for Berea and Fontainebleau sandstones at $L = 300$ μm. The Fontainebleau sample is more homogeneous as indicated by the smaller width of $\mu(\phi,L)$ than that of Berea. The most probable porosity (peak) is close to the average porosity in both cases.

The local percolation probabilities $\lambda(\phi,L)$ (shown as solid lines) are increasing from 0 to 1. This indicates that the measurement cells with higher porosity are more likely to be connected at this length scale in both sandstones. The $\lambda(\phi,L)$ for Berea fall to the left of the corresponding $\mu(\phi,L)$ whereas in Fontainebleau it falls to the right. This indicates that the degree of connectivity of Berea is larger than that of Fontainebleau sandstone.

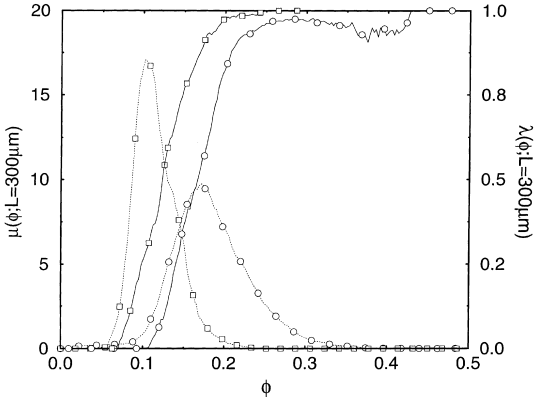


Fig. 2. Local porosity distribution $\mu(\phi,L)$ (dotted lines) and local percolation probability $\lambda(\phi,L)$ (solid lines) for Berea sandstone (circles) and Fontainebleau sandstone (squares) for the measurement cell size $L = 300$ μm. The ordinate for the graphs of $\mu(\phi,L)$ is on the left and the ordinate for $\lambda(\phi,L)$ is on the right as indicated by the axis labels.

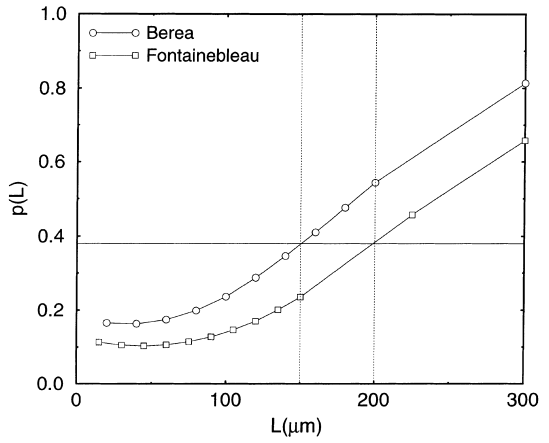


Fig. 3. The total fraction of percolating cells for Berea and Fontainebleau sandstones. The horizontal solid line is $p = 0.38$. The left dotted line represents $\hat{L}_B = 150$ μm, the right one for $\hat{L}_F = 200$ μm.

The difference in the degree of connectivity is more quantitatively evident in Fig. 3, where we have plotted the total fraction of the percolating cells for both the sandstones together. Over the whole range of length scales the connectivity indicator $p(L)$ for Berea is roughly 10% higher than for Fontainebleau. Therefore Berea is expected to have higher conductivity than the Fontainebleau sample.

For given permittivities $\epsilon_{\mathbb{P}} = 87.74$ and $\epsilon_{\mathbb{M}} = 4.7$ (in units of $\epsilon_0 = 8.854 \times 10^{-12}$ F/m), and conductivities $\sigma_{\mathbb{P}} = 1.0\ \mathrm{S \cdot m^{-1}}$ and $\sigma_{\mathbb{M}} = 0.0$ we have computed effective electrical permittivities $\epsilon_{\mathrm{eff}}$ and effective electrical conductivities $\sigma_{\mathrm{eff}}$ in three ways: first we solve Eqs. (8)–(10) exactly, then we solve Eq. (16), and finally we compute $\sigma_{\mathrm{eff}}$ and $\epsilon_{\mathrm{eff}}$ within the EMA.

We solve Eqs. (8)–(10) *exactly* by a finite volume technique [13], the mesh sizes are equal to the resolution $a$. We apply a potential gradient across the sample and require no flow boundary conditions on the other faces of the sample. On the stochastic internal boundary $\partial\mathbb{P}$ we have continuity of normal components of the electric displacement $\mathbf{D}(\mathbf{r})$ and tangential components of the electric field $\mathbf{E}(\mathbf{r})$. For the permittivity problem we calculate $\epsilon_{\mathrm{EC}}$ from Eq. (11). For the electrical conductivity problem we solve a similar set of equations with values $\sigma_{\mathbb{P}}$ and $\sigma_{\mathbb{M}}$ above.

We compute $\sigma_{\mathrm{LPT}}(L)$ and $\epsilon_{\mathrm{LPT}}(L)$ as functions of $L$ by solving the approximate Eq. (16) iteratively. As suggested by Boger et al. [4], we find a length scale $\hat{L}$ (see Table 1) such that $\epsilon_{\mathrm{LPT}}(\hat{L}) = \epsilon_{\mathrm{EC}}$. The results $\hat{L}_B = 150$ μm for Berea and $\hat{L}_F = 200$ μm for Fontainebleau form the last column in Table 1. Thus $\hat{L}$ may be interpreted as an electrical length which can be used to characterize the electrical transport properties.

We observe also that the line $p = 0.38$ in Fig. 3 intersects the $p_B(L)$ at $\hat{L}_B$ and $p_F(L)$ at $\hat{L}_F$. This supports the interpretation from above that the length scale $\hat{L}$ is related to the connnectivity of the underlying microstructure. It is also gratifying to observe that $\hat{L}$ is approximately two times the correlation length, because this ensures that the local geometries are statistically independent as required in Section 4. However, we cannot rule out the dependence of $\hat{L}$ on other structural properties of the sandstones. Further work on different sandstones is necessary to establish any such relationship (Table 2).

Finally we calculate the effective conductivity $\sigma_{\mathrm{EMA}}$ and permittivity $\epsilon_{\mathrm{EMA}}$ also within the classical EMA [6]

$$\bar{\phi}\frac{c_{\mathbb{P}} - c_{\mathrm{eff}}}{c_{\mathbb{P}} + 2c_{\mathrm{eff}}} + (1 - \bar{\phi})\frac{c_{\mathbb{M}} - c_{\mathrm{eff}}}{c_{\mathbb{M}} + 2c_{\mathrm{eff}}} = 0. \tag{17}$$

This equation can be obtained as the special case $L = 0$ from Eq. (16). We find that $\sigma_{\mathrm{EMA}} = 0$, because the porosity $\bar{\phi}$ of both the samples is below the percolation threshold $\bar{\phi}_c = 1/3$. For both the sandstones, $\epsilon_{\mathrm{LPT}}$ for $L = \hat{L}$ is in better agreement

Table 2
Effective electrical permittivity $\epsilon$ (in units of $\epsilon_{\mathbb{P}}$) and effective electrical conductivity $\sigma$ in $\mathrm{S \cdot m^{-1}}$

| Samples | $\epsilon_{\mathrm{EC}}$ | $\epsilon_{\mathrm{LPT}}$ | $\epsilon_{\mathrm{EMA}}$ | $\sigma_{\mathrm{EC}}$ | $\sigma_{\mathrm{LPT}}$ | $\sigma_{\mathrm{EMA}}$ |
|---|---|---|---|---|---|---|
| Berea | $0.1121 \pm 0.0016$ | 0.1235 | 0.0931 | $0.0240 \pm 0.0026$ | 0.0198 | 0 |
| Fontainebleau | $0.0934 \pm 0.0021$ | 0.0953 | 0.0763 | $0.0136 \pm 0.0043$ | 0.0106 | 0 |

with $\epsilon_{EC}$ than the corresponding $\epsilon_{EMA}$. It should be emphasized that $\sigma_{LPT} > 0$ while $\sigma_{EMA} = 0$. This is important for the transport properties of rocks, because generally rocks are connected down to very low porosity (even below 1%).

In summary we have studied the quantitative prediction of macroscopic material properties in the simplest linear example. Despite its simplicity the disordered potential equation has numerous other applications, such as diffusion, heat transport, thermal and electrical osmosis, or hydrodynamic flow to name only a few of them. For the quantitative prediction of mechanical properties such as elastic moduli we are currently extending LPT to the case of linear elasticity. We feel that a quantitative understanding of the influence of the microstructure on linear response properties is a prerequisite without which predictive theories of nonlinear phenomena such as plasticity and fracture will remain limited in their applicability to experiment.

## Acknowledgements

The authors gratefully acknowledge Dr. P.E. Øren (Statoil), Dr. S. Bakke (Statoil) for providing the sample data sets, and thank the Deutsche Forschungsgemeinschaft for financial support. J.W. is grateful to Dr. S. Schwarzer, Dr. H.-G. Matuttis and Prof. Dr. P. Sheng for discussions, and to the Graduiertenkolleg ''Modellierung und Diskretisierungsmethoden für Kontinua und Strömungen'' for financial support.

## References

[1] M.J. Beran, Statistical Continuum Theories, Interscience Publishers, New York, 1968.
[2] B. Biswal, C. Manwart, R. Hilfer, Three-dimensional local porosity analysis of porous media, Physica A 225 (1998) 221.
[3] C. Böttcher, Theory of Electric Polarization, vol. I, Elsevier, Amsterdam, 1973.
[4] F. Boger, J. Feder, T. Jøssang, R. Hilfer, Microstructural sensitivity of local porosity distributions, Physica A 187 (1992) 55.
[5] C.F. Bohren, D.R. Huffman, Absorption and Scattering of Light by Small Particles, Wiley, New York, 1983.
[6] D.A.G. Bruggeman, Berechnung verschiedener physikalischer Konstanten von heterogenen Substanzen. I. Dielektrizitätskonstanten und Leitfähigkeiten der Mischkörper aus isotropen Substanzen, Ann. Phys. 24 (1935) 636.
[7] R.M. Christensen, Mechanics of Composite Materials, Wiley, New York, 1979.
[8] R. Hilfer, Geometric and dielectric characterization of porous media, Phys. Rev. B 44 (1991) 60.
[9] R. Hilfer, Local porosity theory for electrical and hydrodynamical transport through porous media, Physica A 194 (1993) 406.
[10] R. Hilfer, Transport and relaxation phenomena in porous media, Adv. in Chem. Phys. XCII (1996) 299.
[11] R. Hill, A self-consistent mechanics of composite materials, J. Mech. Phys. Solids 13 (1965) 213.
[12] J.D. Jackson, Klassische Elektrodynamik, de Gruyter, Berlin, 1983.
[13] J.J.I.M. van Kan, A. Segal, Numerik partieller Differentialgleichungen für Ingenieure, B.G. Teubner, Stuttgart, 1995.
[14] T. Mura, Micromechanics of Defects in Solids, Martinus-Nijhoff, Dordrecht, 1987.
[15] T. Mura, G.J. Weng, Micromechanics and Inhomogeneity: the Toshio Mura 65th Anniversary Volume, Springer, Heidelberg, 1990.
[16] P. Sheng, Introduction to Wave Scattering, Localization, and Mesoscopic Phenomena, Academic Press, San Diego, 1995.